International Journal of Nanomedicine

Dovepress
open access to scientific and medical research

Open Access Full Text Article

ORIGINAL RESEARCH

Interaction Between Ropivacaine and a Self-Assembling Peptide: A Nanoformulation for Long-Acting Analgesia

Fei Peng[1], Jing Liu[1,2], Yujun Zhang[1,2], Guoyan Zhao[1,2], Deying Gong[1,2], Liu He[1,2], Wensheng Zhang[1,2], Feng Qiu[1,2]

[1]Laboratory of Anesthesia and Critical Care Medicine, Department of Anesthesiology, Translational Neuroscience Center, West China Hospital, Sichuan University, Chengdu, 610041, People's Republic of China; [2]National-Local Joint Engineering Research Center of Translational Medicine of Anesthesiology, West China Hospital, Sichuan University, Chengdu, 610041, People's Republic of China

Correspondence: Feng Qiu; Wensheng Zhang, Email fengqiu@scu.edu.cn; zhang_ws@scu.edu.cn

Introduction: Ropivacaine as a conventional local anesthetic has been used more and more frequently in the treatment of postoperative pain, but its analgesic effect can only last for several hours. In order to fulfill the clinic requirement for long-term analgesia, a long-acting ropivacaine nanocrystal formulation was fabricated through the interaction between ropivacaine and a self-assembling peptide.

Methods: Transmission electron microscopy, dynamic light scattering, circular dichroism and fluorescence spectrometry were used to examine the structural changes caused by the interaction between ropivacaine and the peptide. Scanning electron microscopy, dynamic light scattering, Fourier transform infrared spectrometry, X-ray diffraction and optical microscopy were used to characterize the ropivacaine-peptide nanocrystal. In vitro drug release and pharmacokinetics study were conducted to evaluate the slow-release profile of the nanocrystal formulation. A rodent cutaneous trunci muscle reflex model was used to evaluate the nociceptive blockade effects, and histological analysis was used to evaluate the local toxicity. A rodent plantar incisional pain model was used to evaluate the analgesic effect.

Results: Soluble ropivacaine monomers interacted with the Q11 peptide through π-π stacking and remolded its self-assembling structure, leading to the formation of drug/peptide nanoparticles which could be mineralized to form drug/peptide nanocrystals by adjusting the pH. Under physiological condition, the nanocrystals could release free ropivacaine slowly. As evaluated in rodent models, the anesthetic and analgesic effects of this formulation were significantly extended without causing toxicity.

Conclusion: Based on the interaction between ropivacaine and Q11, a controllable biomineralization process could be induced to obtain homogeneous nanocrystals, which could be used as an injectable long-acting analgesic formulation. This crystallization strategy utilizing the peptide-drug interaction also provided a promising pathway to fabricate long-acting formulations for many other small molecular drugs.

Keywords: self-assembling peptide, nanocrystal, local anesthetics, π-π stacking, slow release, long-acting analgesia

Introduction

In the treatment of perioperative or chronic pain, local anesthetics (LAs) such as lidocaine, bupivacaine and ropivacaine have been widely used to avoid or reduce the consumption of opioid, which could cause some side effects such as nausea, vomiting, habituation and addiction.[1,2] However, the duration of LAs is often limited by their short half-lives. Since nearly all LAs are used in their soluble hydrochloride form, they tend to be absorbed and cleared very quickly in vivo. Therefore, the effect of a single injection of most LAs can last only several hours, which is insufficient to meet current clinical requirements for long-time operation or postoperative analgesia.[3] Recently, carrier materials such as liposomes,[4] lipid-polymer hybrid nanoparticles,[5] and hydrogel/microsphere composite[6] have been used to encapsulate LAs for developing long-acting formulations. However, encapsulated LAs as small water-soluble molecules still tend to leak out from the carriers quickly, so that these conventional materials usually achieved limited efficacy in controlling the drug release rate.

Received: 6 April 2022
Accepted: 22 July 2022
Published: 29 July 2022

Self-assembling peptides (SAPs) are a category of nanomaterials featured by generating diverse types of nanostructures with tunable functionality. In the past two decades, SAPs have been widely used for drug delivery through a variety of strategies including hydrophobic encapsulation, electrostatic absorption, chemical conjugation and hydrogel embedding.[7–9] For example, SAPs have been used to encapsulate small molecular hydrophobic drugs through hydrophobic interaction to increase their bioavailability.[10–12] Moreover, some drugs embedded in SAP hydrogels could acquire a much slower and controllable release profile by binding with the SAP nanofibers through electrostatic or hydrophobic interaction.[13,14] Alternatively, Ashwanikumar et al[15] designed a SAP containing phenylalanine residues to entrap 5-fluorouracil through π-π stacking, suggesting a special slow-release strategy for drugs containing aromatic groups. Interestingly, many SAPs such as Q11, FEFEFKFK and FHFDFHFD also contain multiple phenylalanine residues in their sequences,[16–18] meanwhile nearly all LAs used in clinic contain a 2,6-dimethylbenzene aromatic group. This makes it possible to encapsulate LAs with these phenylalanine-containing SAPs through π-π stacking, which is expected to improve their slow-release profile.

In the past two decades, ropivacaine hydrocholoride (RH) has been used more and more frequently in clinic because of its longer duration than lidocaine hydrocholoride and lower toxicity than bupivacaine hydrocholoride.[19] However, the analgesic effect of RH could last only several hours because of its small molecule weight and high water-solubility.[20] Aiming to prolong the duration of current ropivacaine formulation, in this study we used Q11, a SAP containing phenylalanine residues, to encapsulate RH. Interestingly, we found that rather than simply being embedded by Q11 nanofibers, RH could extensively interact with Q11 and change its self-assembling behavior, leading to the formation of drug/peptide nanoparticles. Based on this finding, a biomineralization process was induced by pH adjustment to obtain ropivacaine-Q11 nanocrystals, which exhibited significantly slowed drug release rate and prolonged analgesic duration.

Materials and Methods

The Transmission Electron Microscopy (TEM) Observation

Lyophilized powder of Q11 peptide (with sequence of QQKFQFQFEQQ, M.W. 1526.63 Da) with purity over 95% was commercially synthesized by Bootech BioScience & Technology Co., Ltd. (CN). RH (M.W. 328.88 Da) was purchased from Sigma-Aldrich (US). Stock solutions of 2 mM Q11 and 20 mM RH were prepared by dissolving the powders in Milli-Q water. The Q11 stock solution was mixed with an equal volume of Milli-Q water or RH stock solution to obtain 1 mM Q11 with or without 10 mM RH. To observe the self-assembling structure of Q11 by TEM, 10 μL of each sample was set on the surface of a 400-mesh copper grid for 2–5 minutes to deposit the sample, after which a piece of filter paper was used to blot the peptide solution. The sample was negatively stained with 10 μL of 2% phosphotungstic acid for about 2 min. Finally, the staining solution was blotted with filter paper and the grid was air-dried. The grids were imaged using a Tecnai G2 F20 transmission electron microscope (FEI, US).

The Dynamic Light Scattering (DLS) Analysis

Q11 solutions with or without RH prepared above were used for DLS study. The hydrodynamic diameters of the two samples were measured using a NanoBrook Omni particle size analyzer (Brookhaven Instruments Corporation, USA). Each reported hydrodynamic diameter with a polydispersity index (PDI) was the averaged result from 6 different measurements, and each measurement was composed of 10 rounds of collections.

The Circular Dichroism (CD) Analysis

Q11 solution (0.4 mM) was mixed with an equal volume of Milli-Q water or RH solution at different concentrations (0.4–4 mM) to obtain RH/Q11 mixtures. Each sample contained 0.2 mM Q11 and RH at different concentrations. The CD spectra of all samples were measured using a Chirascan plus CD spectrophotometer (Applied Photophysics, UK). Briefly, each sample was filled into a quartz cuvette with a path length of 0.2 cm, and CD signal between 200–260 nm was measured 3 times to get an averaged spectrum.

Measurement of Auto-Fluorescence

The auto-fluorescence of Q11 (1 mM), RH (10 mM) and the RH/Q11 mixture containing 1 mM Q11 and 10 mM RH were measured with a Fluorolog spectrofluorometer (Horiba scientific Inc., US). Fluorescent spectra between 460–600 nm were collected with the excitation wavelength of 450 nm.

Preparation of Ropivacaine Crystal and Ropivacaine-Q11 Crystal

The pH of 10 mM RH solution and RH/Q11 mixture containing 10 mM RH and 1 mM Q11 were adjusted to 7.4 by adding 1 M NaOH, and the solutions were held at room temperature for 2 hours, leading to the formation of crystal suspensions. The suspensions were treated in an ultrasonic bath for 20 minutes and centrifuged at 10,000 g for 10 minutes to separate the supernatants and the sediments. The sediments were lyophilized to obtain the ropivacaine crystal (RC) and ropivacaine-Q11 crystal (RQC), respectively. The hydrodynamic diameter of RC and RQC resuspended in water were determined using the DLS method as described above.

The content of ropivacaine and Q11 in RQC was determined by reversed-phase high performance liquid chromatography (HPLC) using an Agilent Extend C18 column (4.6 × 150 mm, 5 μm). Briefly, 10 μL of supernatant separated from the RH/Q11 mixture as described above was injected to an LC-20AD HPLC system (Shimadzu Corporation, Japan) to determine the contents of free ropivacaine and Q11, and the contents of crystalized ropivacaine and Q11 in RQC were calculated accordingly. The loading capacity (LC) and encapsulation efficiency (EE) of RQC were calculated respectively using following equations:

$$\mathrm{LC} = \frac{M_{Ropi}}{M_{Ropi} + M_{Q11}} \times 100\% \ ;$$

$$\mathrm{EE} = \frac{M_{Ropi}}{M_{tRopi}} \times 100\%$$

where M_{Ropi} and M_{Q11} were the amounts of ropivacaine and Q11 in RQC as calculated from the HPLC results, and M_{tRopi} was the total amount of ropivacaine added in the initial mixtures before crystallization.

The Scanning Electron Microscopy (SEM) Observation

For morphological study using SEM, RC and RQC obtained above were spread on glass slides and coated with gold using a 108 Auto sputter coater (Cressington Scientific Instruments, UK). The slides were observed using an EVO 10 scanning electron microscope (ZEISS, DE). Alternatively, Q11 solution (1 mM) was dropped onto a glass slide and freeze-dried, which was coated with gold and observed using SEM as described above.

The Fourier Transform Infrared (FT-IR) Spectra Measurement

To inspect the FT-IR spectra of RQC, RC, RH and Q11, the dry powder of each sample was spread on zinc selenide substrate, and the FT-IR spectra were collected using a Nicolet 6700 spectrometer (Thermo Scientific Inc., USA).

The X-Ray Diffraction (XRD) Analysis

The XRD patterns of RQC, RC, RH and Q11 were examined to compare their crystal structures. The dry powder of each sample was placed on a sample holder and the measurement was conducted with an Empyrean X-ray diffractometer (PANalytical, NL) using Cu Kα radiation (λ=1.54 Å).

The X-Ray Photoelectron Spectroscopy (XPS) Analysis

XPS measurement and high-resolution scans were collected with a Kratos Axis ULTRA X-ray photoelectron spectrometer (Kratos, UK). The measurement was carried out at power of 15 kV and electrical current of 5 mA. Survey spectra were collected with pass energy of 160 eV. High-resolution scans were taken with pass energy of 20 eV. The high-resolution spectra for N 1s were fitted using CasaXPS software (Version 2.3.19).

Optical Microscope Imaging

Thioflavin-T (ThT) powder was purchased from Sigma-Aldrich Co. (US) and 1 mM ThT stock solution was prepared by dissolving the powder in Milli-Q water and passing it through a 0.22 μm filter. To confirm the existence of Q11 peptide in RQC, resuspended RQC powder was spread on a glass slide and stained with diluted ThT solution (10 μM) for 10 min. The ThT-stained sample was imaged with an Olympus BX51 fluorescence microscope (Olympus, JP).

To visualize the structural details of the drug-peptide crystal, doxorubicin (DOX) was used as a substitute for ropivacaine to obtain drug-peptide nanocrystals. Similar to the crystallization process of RQC described above, DOX-Q11 crystal (DQC) was acquired by increasing the pH of the mixture containing 10 mM doxorubicin hydrochloride and 1 mM Q11. The DQCs were spread on a glass slide, stained with ThT (10 μM) for 10 minutes and imaged using an A1RMP+ two-photon laser-scanning confocal microscope (Nikon, JP).

In vitro Drug Release Study

RH powder was dissolved in Milli-Q water to get 0.75% RH solution. RC and RQC obtained above were resuspended by PBS respectively to acquire suspensions with a ropivacaine concentration of 5%. The RH, RC and RQC formulations were used for the drug release study and consequential experiments in vivo.

The drug release profile was investigated using a dialysis method. Each sample (1 mL) was placed in a Spectra/Por Float-A-Lyzer G2 dialysis device (1 mL, 8–10 kDa MWCO, Spectrum labs, US) and dialyzed with 30 mL of PBS. At each time point, 15 mL of the sample was withdrawn from the dialysis device, following which 15 mL of fresh PBS was added. The amount of released ropivacaine at each time point was determined by the HPLC method as described above and the cumulative amount of released ropivacaine was calculated, which was converted to the percentage cumulative release rate of the total ropivacaine amount. Three parallel repeats were set for each formulation, and the drug release profiles were constructed by plotting the cumulative ropivacaine release rate against time.

Animals

Specific pathogen free female Sprague-Dawley rats (250–350 g) were purchased from Dossy Experimental Animal Co., LTD (CN) and housed in cages in a 6 a.m. to 6 p.m. light-dark cycle. All animal study protocols were approved by the Institutional Animal Care and Use Committee at West China Hospital of Sichuan University (Ethical approval number, 2019302A) and conducted in strict accordance with the Guide for the Care and Use of Laboratory Animals by the United States National Institutes of Health.

Pharmacokinetics Study

The rats were randomly divided into three groups and received subcutaneous injection of 0.5 mL of different formulations including 0.75% RH, RC and RQC containing 5% ropivacaine (n=6). Blood samples (0.4 mL for each collection) were collected from the tail vein at set time points following injection and centrifuged at 3000 g for 10 minutes to get the plasma. Then 150 μL of acetonitrile containing 10 ng/mL prilocaine as internal standard was added to 50 μL of each sample, and the mixture was vortexed and centrifuged at 20,000 g for 10 minutes to collect the supernatant. Each sample was analyzed by liquid chromatography-mass spectrometry (Agilent 1260–6460, Agilent Technology, US).

An Agilent Extend C18 column (3 × 100 mm, 3.5 mm) with a mobile phase of solvent A (water containing 0.05% formic acid) and solvent B (acetonitrile) was used for the chromatographic separation. The flow rate was 0.3 mL per minute, and the column temperature was 35 °C. The gradient was set as follows: 17% B to 22% B for 3 minutes, then to 95% B within 0.1 minute and hold for 2 minutes. The positive ion mode (ESI+) and multiple reaction monitoring modes were used for mass spectrometric analysis. The capillary temperature was 350 °C, and the spray voltage was 3500 V. The pharmacokinetic parameters of different formulations were analyzed using a Drug and Statistic Version 3.0 (DAS 3.0) software (the Mathematical Pharmacology Committee, Chinese Pharmacological Society, CN).

Evaluation of Anesthetic Efficacy

The anesthetic efficacy of different ropivacaine formulations was evaluated on a cutaneous trunci muscle reflex (CTMR) model as previously described.[21] The rats were randomly divided into different groups including 0.75% RH, RC or RQC formulations containing 5% ropivacaine (n=6). Animals in each group received a subcutaneous injection of 0.5 mL of corresponding formulation on shaved dorsal skin, and the wheal formed at the injection site was marked along its edge. Six pinpricks were randomly applied on the marked skin using a 26-gauge needle. Pinpricks causing a CTMR were recorded as positive and the number of positive responses was converted to a nociceptive blockade score.

Histological Analysis

The rats were randomly divided into different groups including RH, RC and RQC, which received a subcutaneous injection of 0.5 mL of 0.75% RH, RC or RQC containing 5% ropivacaine, respectively (n=6). The rats were humanely euthanized on day 7 or day 14 after the injection, and the subcutaneous tissues at the injection site were collected to evaluate local toxicity. The isolated tissues were fixed in 10% formalin solution for 48 hours and dehydrated with 70–100% ethanol. Paraffin-embedded sections were prepared and stained with hematoxylin-eosin. The photomicrographs of stained sections were imaged using a BA210 digital microscope (Motic company, CN). A histological scoring system was used to evaluate the inflammation grade as previously described.[22]

Efficacy Evaluation in Incisional Pain Model

A rodent incisional pain model was used to evaluate the analgesic efficacy of different formulations as previously described.[23] The rats were randomly divided into four groups (n=6) and received general anesthesia by isoflurane. For each mouse, the plantar of the left-hind paw was surface-sterilized with iodophor and a longitudinal incision of 1 cm was made through the skin and underlying fascia of the plantar surface, starting at 0.5 cm from the heel proximal edge and extending toward the toes. The plantaris muscle was then exposed, and a longitudinal incision was created, keeping the muscle origin and insertion site intact. The skin was sutured after hemostatic compression, following which 50 μL of 0.75% RH, RC or RQC containing 5% ropivacaine, or normal saline (NS) as the control was immediately injected around the incision. Mechanical nociceptive thresholds in response to mechanical stimuli were assessed using von Frey filaments. The von Frey filaments were applied vertically in a progressively increasing manner with bending forces of 0.4, 0.6, 1, 1.4, 2, 4, 6, 8, 10, 15 g to an area adjacent to the incision. The investigator used just enough pressure to bend the filament gently until the lowest bending force that produced withdrawal of the hind paw was reached, which was recorded as the paw withdrawal threshold (PWT). Otherwise, for rats without a paw withdrawal reaction, a cut-off bending force of 15 g was recorded. Each application was maintained for 5 seconds or until paw lifting/licking (positive withdrawal response) was observed. The PWT was measured 1 day before the incision was created and repeated at different time points following the injection of drugs.

Meanwhile, the cumulative pain scores (CPS) were also evaluated as previously described.[24] The left hind paws of the rats were observed and the score was recorded as follow: 0 point was given if the incised paw touched the mesh while the wound was blanched or distorted; 1 point was given if the wound touched the mesh without blanching or distorting; 2 points were given if the incised paw did not touch the mesh. Scores were continuously recorded every 5 minutes for an hour, and the sum of the 12 scores (0–24) were added to obtain the CPS.

Statistical Analysis

All experiments were repeated at least three times, and the results were shown as the means ± standard deviation. All statistical analyses were conducted via one-way ANOVA using GraphPad Prism software (version 5.01).

Results and Discussion

Interaction Between Q11 Nanofibers and Ropivacaine

Q11 peptide self-assembling into orderly nanofibers has been extensively investigated as an immune adjuvant for developing peptide vaccines because of its excellent biocompatibility and biodegradability.[25–27] However, unlike other

peptide nanofiber materials, the capability of Q11 nanofibers to deliver small molecule drugs has not been exploited. There are six glutamine residues and three phenylalanine residues in the sequence of Q11 (Figure 1A), which can drive self-assembly of the peptide through hydrophobic interaction and π-π stacking force.[28,29] TEM image in Figure 1C clearly shows the nanofibril structure of Q11 as previously reported.[30]

Surprisingly, after Q11 was mixed with RH, the mixture formed typical nanoparticles, which was significantly different from the nanofiber structures of Q11 (Figure 1C). Meanwhile, as shown in Figure 1D, the average size of Q11 measured by DLS was 564.1 ± 55.8 nm (PDI = 0.470), while the average size of RH/Q11 was 91.5 ± 9.6 nm (PDI = 0.289). These DLS results also indicate the transformation from inhomogeneous nanofibers to smaller and more homogeneous nanoparticles when Q11 was combined with RH. It seemed that there were some strong interactions between Q11 and RH molecules, which drastically changed the self-assembling behavior of Q11.

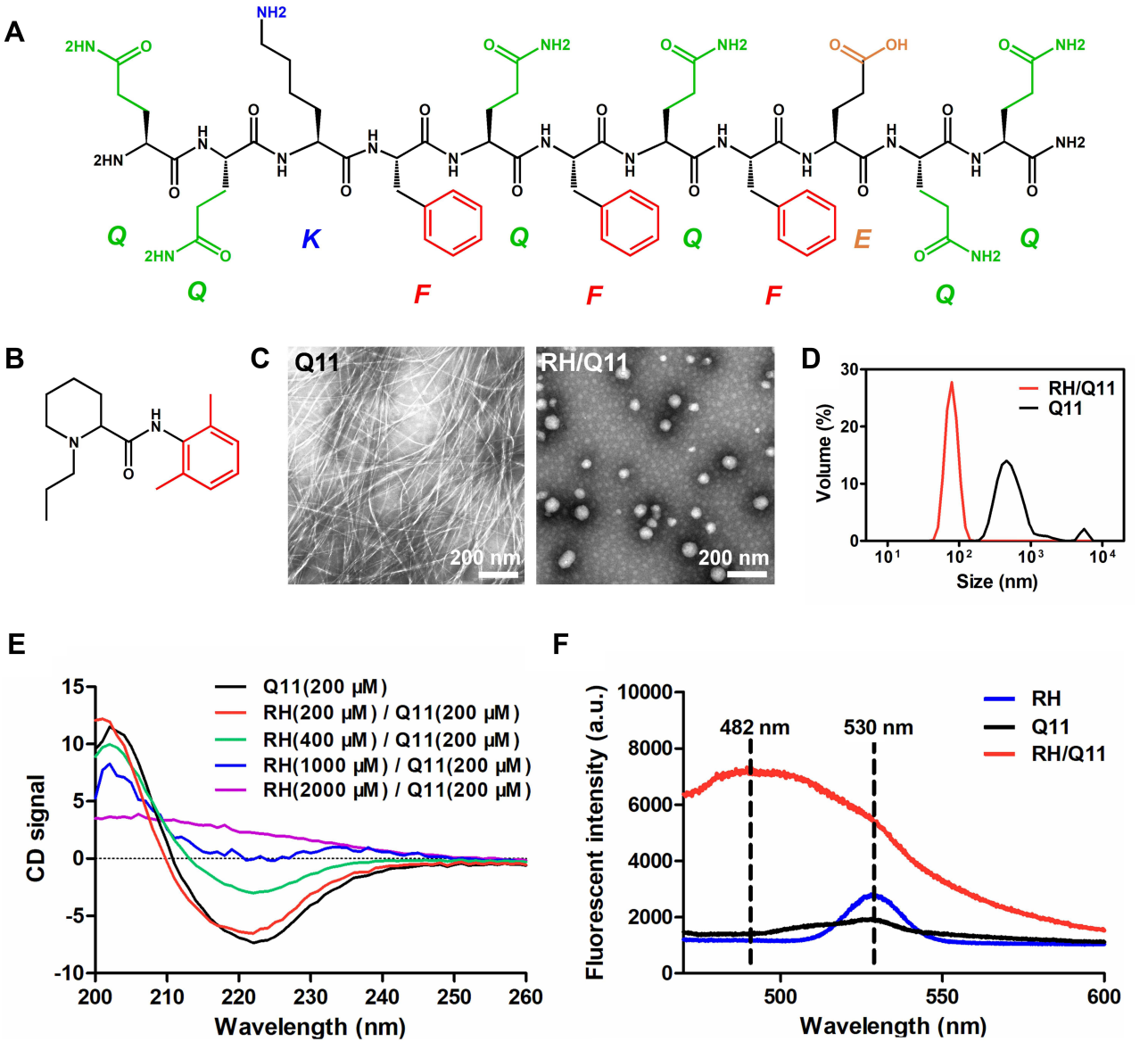

Figure 1 Q11 interacts with ropivacaine and forms nanoparticles. (**A**) The chemical structure of the Q11 peptide. (**B**) The chemical structure of ropivacaine. (**C**) TEM images of nanofibers formed by Q11 and nanoparticles formed by RH/Q11 mixture with molar ratio of 10:1. (**D**) Size distribution of Q11 and RH/Q11 mixtures. (**E**) CD spectra of Q11 and RH/Q11 mixtures with different RH concentrations. (**F**) Auto-fluorescent spectra of RH, Q11 and RH/Q11 with excitation wavelength of 450 nm. Q11 concentration was 1 mM and RH concentration was 10 mM.

As reported by many previous studies, Q11 self-assembled into nanofibers based on orderly β-sheet conformation.[31–33] As shown in Figure 1E, CD spectrum for pure Q11 exhibited a positive peak around 205 nm and a negative peak around 220 nm, which indicated the existence of typical β-sheet secondary structure.[34] However, as the concentration of RH in RH/Q11 mixture was increased, the peptide gradually lost its β-sheet signal. When the ratio of RH: Q11 reached 10:1, the peptide showed no β-sheet peaks at all. These results suggest that the interaction between RH and Q11 drastically changed the peptide's secondary structure, which might lead to the transition of self-assembling structures from nanofibers to nanoparticles.

Since ropivacaine contains a dimethylbenzene group (Figure 1B) and Q11 contains three phenylalanine residues, it is possible that π-π stacking force can be formed between their phenyl rings and links the two molecules together.[35,36] The existence of π-π stacking force can be proved by the auto-fluorescent spectrum for RH/Q11 mixture shown in Figure 1F. RH or Q11 alone exhibited a weak fluorescence peak around 530 nm, while the RH/Q11 mixture exhibited an enhanced fluorescence peak around 482 nm, which could be attributed to the orderly interaction of π-π stacking.[37]

As shown in Scheme 1, it is proposed that as dimethylbenzene groups of RH molecules competitively bind with the phenyl ring of phenylalanine residues on Q11 through π-π stacking, regular Q11 nanofibers are gradually disassembled as the peptide loses its β-sheet structure. However, the peptide chains can still crosslink with each other, probably through the hydrophobic interaction between the side chains of glutamines as previous described.[12,38] Without the support of orderly β-sheet structure, the crosslink finally leads to the formation of nanoparticles.

It has been known that when the pH of a pure RH solution is elevated, the molecule became deprotonated and less soluble, which could lead to the mineralization of ropivacaine and the formation of crystals.[39] However, this process is hard to control without preformed nanostructures as nucleus, so that pure RH usually produces large crystals with limited anesthetic efficacy. In the present study, we suppose that following the formation of nanoparticles in the RH/Q11 mixture as described above, a controllable and homogeneous crystallization process could be induced (Scheme 1). Based on these preformed nanoparticles as nucleus, ropivacaine-Q11 nanocrystals could be acquired by simply increasing the pH of RH/Q11 mixture. These nanocrystals could be further exploited as a slow-release ropivacaine depot, which is expected to achieve prolonged anesthesia and analgesia after injected into animals.

Characterization of RQC

As shown in Figure 2A, the average size of RC measured by DLS is 7730.1 ± 817.6 nm (PDI = 0.481), while the average size of RQC is 634.2 ± 87.7 nm (PDI = 0.289), suggesting that Q11 peptide induced the formation of much smaller and more homogenous crystals. As shown in Figure 2B, RCs were cube-like microcrystals with rigid edges, which were similar to the morphology of many inorganic monocrystals. On the other hand, RQCs obtained from the mixture of ropivacaine and Q11 were nanoparticles with a quite different morphology, which were predominated by sphere-like

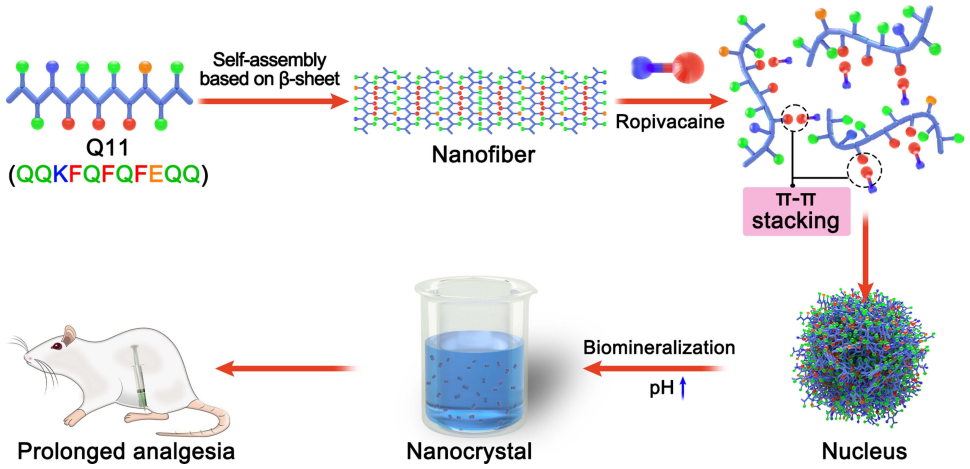

Scheme 1 Schematic illustration of ropivacaine-Q11 interaction and the formation of injectable long-acting formulation by the biomineralization process based ropivacaine-Q11 nanoparticles.

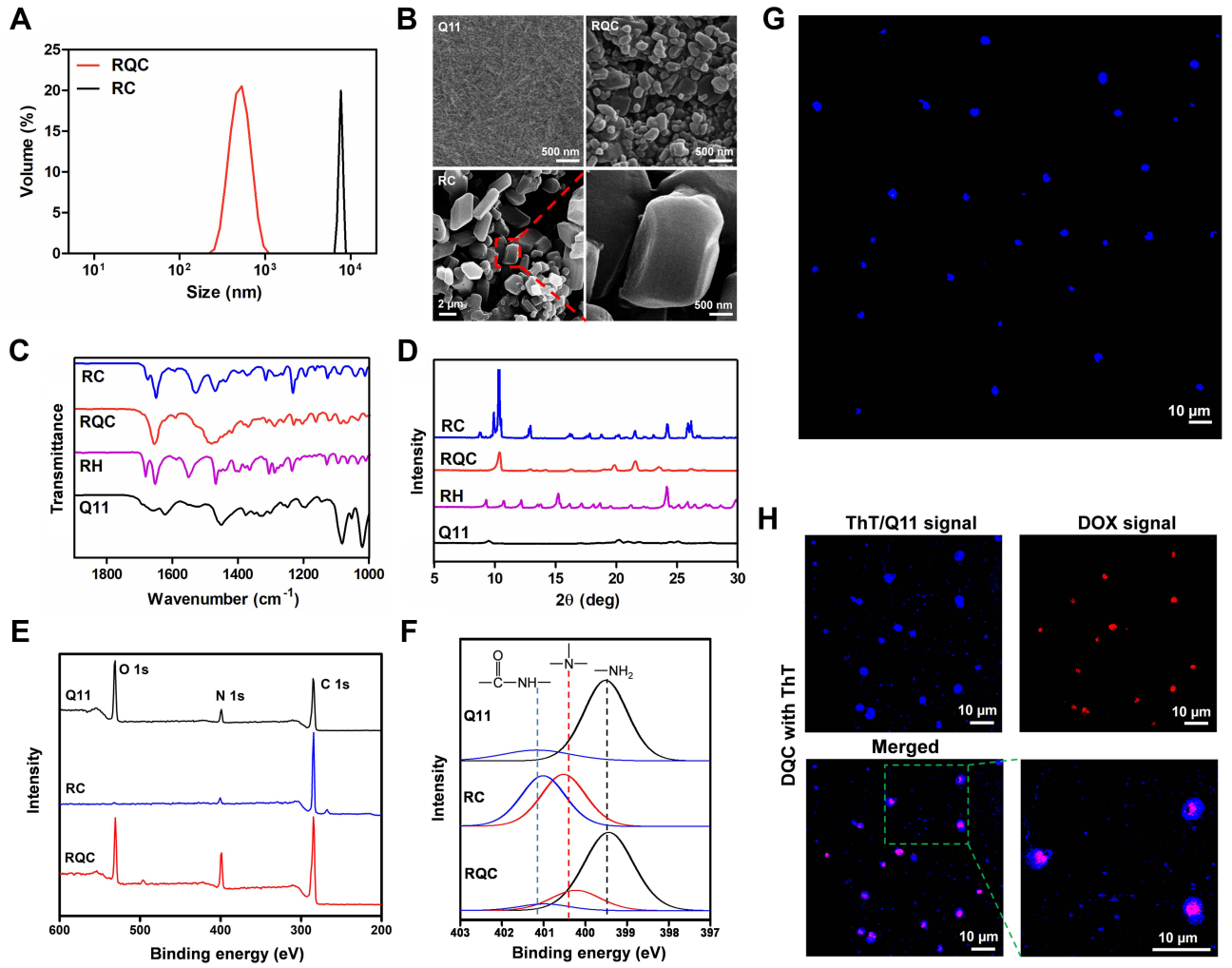

Figure 2 Characterization of RQC and RC. (**A**) Size distribution of RQC and RC. (**B**) SEM images of Q11, RQC and RC. (**C**) FT-IR spectra of RQC, RC, RH and Q11. (**D**) XRD patterns of RQC, RC, RH and Q11. (**E**) XPS survey spectra of RQC, RC and Q11. (**F**) High-resolution XPS for N 1s spectra deconvolution analysis of RQC, RC and Q11. (**G**) Fluorescence image of ThT-stained RQC. (**H**) Fluorescence images of ThT-stained DQC.

particles with much smaller size. As a comparison, pure Q11 formed a coarse film-like structure on the substrate, indicating the collapse of dense nanofibers scaffold. It is obvious that although by increasing the pH, ropivacaine could always undergo crystallization with or without binding with Q11, preformed RH/Q11 nanoparticles as nucleus could control the crystallization process and lead to the formation of nanocrystals with much smaller size. On the other hand, RH also drastically changed the self-assembling behavior of Q11, leading to the absence of nanofiber scaffolds in the RH/Q11 mixture.

As measured by the HPLC-based method, the loading capacity and encapsulation efficiency of ropivacaine in RQC was 87.9 ± 0.5% and 69.5 ± 0.6%, respectively. In conventional drug loading strategies, drugs are simply encapsulated by the carrier materials, so that the loading capacity is usually limited. While in this strategy, by providing nucleus for controlling the crystallization of the drug, Q11 as the carrier material could only take a very small portion in the final formulation, indicating that the RQC is an efficient drug loading system.

As shown in Figure 2C, the FT-IR spectrum of RQC was quite different from those of RC or Q11 spectrum, which indicated that there were extensive interactions between ropivacaine and Q11 in the crystals. In addition, RQC showed a different XRD pattern compared with RC, which was featured by a sharp decrease of diffraction peak around 10 degrees (Figure 2D). These results further indicate that incorporation of Q11 in RQC greatly changed the crystal structure, which could lead to their different size, morphology and ropivacaine-releasing profile. As shown by the XPS spectra in

Figure 2E, RC generated a weak O 1s signal due to the very low ratio of oxygen in the ropivacaine molecule, while RQC generated a strong O 1s peak close to that of Q11. Meanwhile, the high-resolution N 1s spectra of RQC, RC and Q11 were deconvoluted to compare their composition as previously described.[40] As shown in Figure 2F, typical peaks for amino group and amide group appeared in Q11, typical peaks for amide group and tertiary amine group appeared in RC, while RQC exhibited peaks for all the three groups. The results in both Figure 2E and F could confirm the co-existence of Q11 and ropivacaine in the RQC.

ThT as a specific dye for amyloid-like aggregates was used to stain the RQCs, which could further confirm the existence of Q11 peptide in the crystals. As shown in Figure 2G, RQC stained with ThT showed typical blue ThT-binding fluorescence, which preliminarily proved the existence of Q11 aggregates in the crystal particles. On the contrary, RC showed no ThT-binding fluorescence under the same condition (result not shown). Moreover, DOX as a model drug was used to show the co-localization of drug and Q11 peptide in the nanocrystals. As shown in Figure 2H, fluorescent images clearly indicate that crystallized drugs were embedded in the scaffold of peptide aggregates.

Slow Release of Ropivacaine in vitro and in vivo

As shown in Figure 3A, over 90% of ropivacaine was released from RH in the first 2 hours, and the drug was exhausted after 4 hours. The RC group showed limited slow-release effect compared with the RH group, with 77% of ropivacaine released in the first 2 hours and 84% of ropivacaine released after 4 hours. On the other hand, only 64% of ropivacaine was released from the RQC group in the first 2 hours, and 73% of ropivacaine was released after 4 hours. The RH and RC groups completed the release of ropivacaine after 8 hours and 24 hours, respectively, while ropivacaine release from the RQC group lasted until 48 hours, exhibiting a considerably sustained release profile. The fast release of RH is not surprising, since free ropivacaine in the form of soluble RH could easily diffuse out of the dialysis device. On the contrary, crystallized ropivacaine in RC and RQC groups formed a natural drug depot, which could be dissolved and released out the drug monomers slowly. Additionally, in the RQC group, Q11 formed a coating layer around nanocrystals, which might prevent the direct contact of ropivacaine with the buffer and further slowed down the dissolving process. At the same time, the interaction between Q11 and ropivacaine described above could also inhibit the diffusion of ropivacaine. Based on these mechanisms, the RQC group exhibited a significantly sustained-release profile in vitro.

The changes of plasma ropivacaine concentration at different time points after injection are shown in Figure 3B, which reflect the local release and absorption rate of different ropivacaine formulations in vivo. The time of maximum concentrations of drugs in plasma (T_{max}) was 2 hours for RQC, while the T_{max} of the other two groups was 1 hour. The calculated median elimination half-life ($t_{1/2}$) was 11.9 ± 1.7 hours for RQC, 5.4 ± 1.2 hours for RH and 6.2 ± 1.1 hours for RC, respectively. The calculated mean resident time (MRT) was 13.7 ± 1.3 hours for RQC, 6.5 ± 0.6 hours for RH and 7.7 ± 0.8 hours for RC, respectively. The AUC value was 2202.6 ± 334.4 for RH, 9963.6 ± 933.6 for RC and 10,774.1 ± 632.1 for RQC, respectively. These were in well accordance with their initial dosages given to the animal. Compared with the RQC and the RH groups, the RC group showed a much higher peak concentration, which might

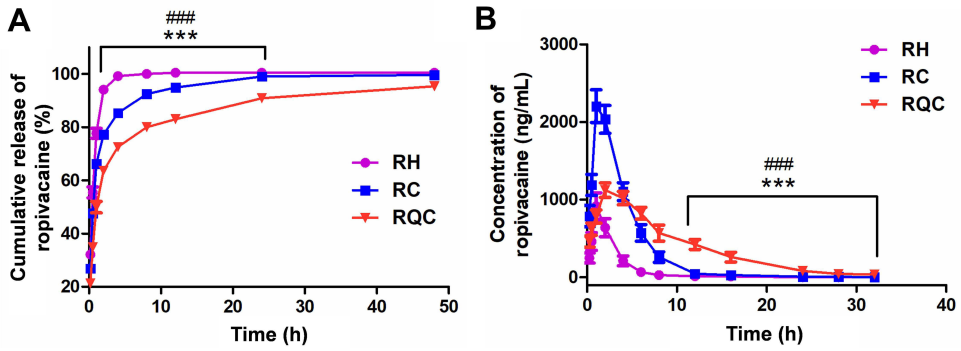

Figure 3 Slow release of ropivacaine in vitro and in vivo. (**A**) Release profile of ropivacaine from different formulations in vitro. (**B**) Pharmacokinetic profiles of different ropivacaine formulations in vivo. The statistical significance is shown: ***p < 0.001 (between RQC and RH); ###p < 0.001 (between RQC and RC) by one-way ANOVA.

increase the risk of systemic side effects. On the other hand, although the total ropivacaine concentration in RQC was much higher than that in the 0.75% RH group, its maximum plasma concentration was only a little higher. Considering that 0.75% RH is a clinically acceptable formulation, the safety of RQC for potential clinical application is also expectable.

Prolonged Nociceptive Blockade Effects

The model of subcutaneous infiltration anesthesia has been commonly used to evaluate the duration of LAs.[41–43] As shown in Figure 4A, all formulations achieved complete nociceptive blockade (score of 100%) within 15 minutes, which corresponded with the onset time of ropivacaine.[44] The score for 0.75% RH group rapidly decreased to 61% after 4 hours and reached 0 within 8 hours, which corresponded with the clinic fact that effective anesthesia caused by soluble RH can only last for several hours. The score for the RC group decreased to 58% after 8 hours and reached 0 within 24 hours, reflecting a moderately prolonged anesthetic effect caused by this formulation. On the other hand, the nociceptive blockade effect of the RQC group

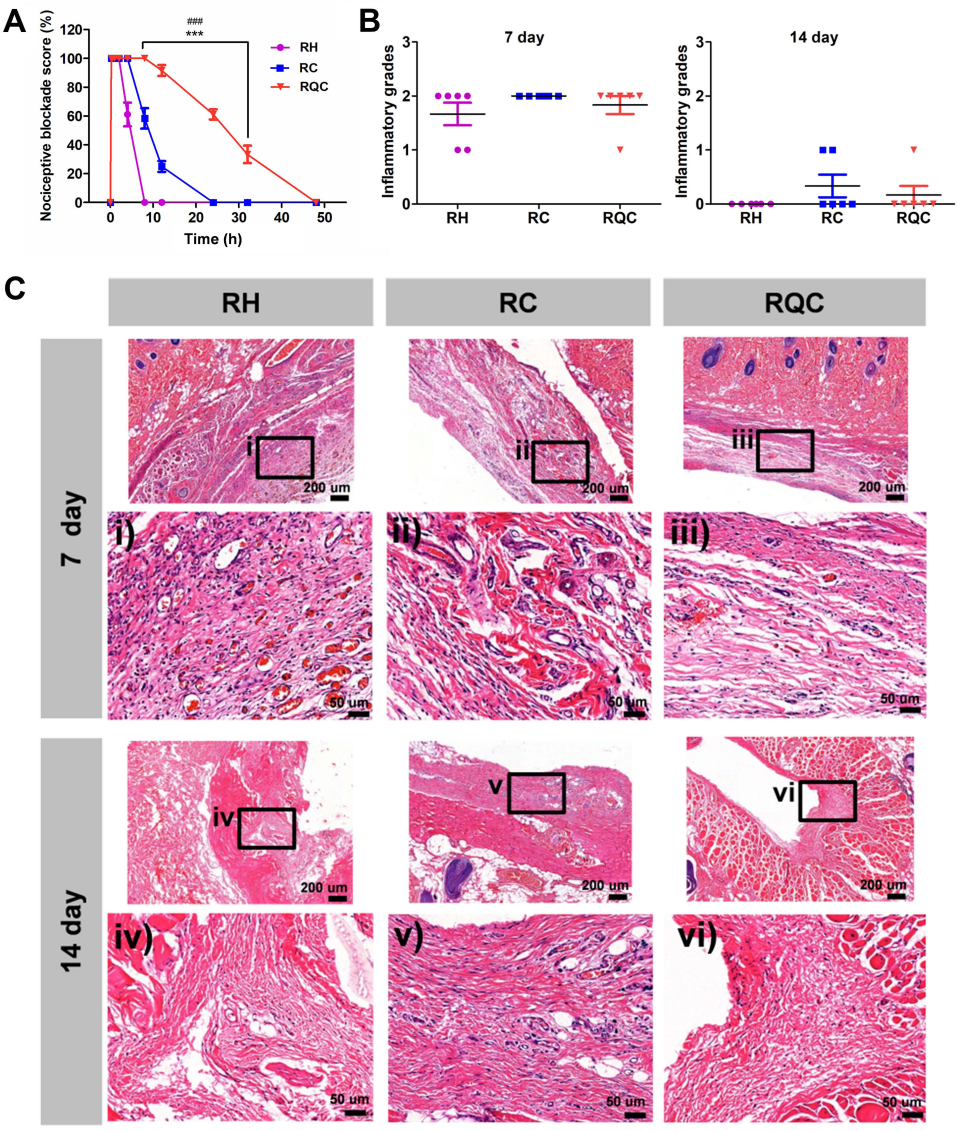

Figure 4 Anesthetic effect of different ropivacaine formulations and their local toxicity. (**A**) Inhibition of the CTMR reflected by nociceptive blockade score. (**B**) Inflammatory grades of the subcutaneous tissue injected with different formulations. (**C**) Photomicrographs of representative H&E-stained sections from tissue at the injection sites. Figures labeled with i to vi at their upper-left corners are the magnified images of areas marked with black squares in corresponding images. The statistical significance is shown: ***$p < 0.001$ (between RQC and RH); $^{###}p < 0.001$ (between RQC and RC) by one-way ANOVA.

decreased slowly and the score remained above 61% after 24 hours, and recorded blockade effect could last for up to 48 hours. These results indicate that RQC has a significantly prolonged anesthetic effect in vivo.

As shown in Figure 4B and C, all formulations showed mild inflammation 7 days after injection, which might be caused by the inherent toxicity of ropivacaine. However, the inflammation associated with all formulations was almost undetectable 14 days after injection, suggesting a recovery from the initial inflammatory damage. These results indicate that similar to the RH formulation used in clinic, the RQC formulation only caused mild and acceptable inflammatory response, which could naturally and gradually recover over time. In addition, these results further demonstrates that the prolonged nociceptive blockade effect of the RQC formulation was caused by sustained drug release instead of severer damage to local tissue.

Combined with the in vitro and in vivo release results described above, it's clear that the prolonged anesthetic effect was caused by the slow release of ropivacaine in the RQC formulation. Although a much higher drug concentration of 5% was used in the RQC formulation, its slow-release profile could maintain the local drug concentration in an effective and safe window. At the same time, the plasma drug concentration was also kept as low as the 0.75% formulation used in clinic, which could avoid the risk of potential systematic toxicity and ensure its safety in clinic applications.

Prolonged Analgesic Effects on Postoperative Pain Model

PWT in response to mechanical stimuli was tested to further evaluate the analgesic effect of different ropivacaine formulations on the postoperative pain model of plantar incision. As shown in Figure 5A, 2 hours after the surgery, the PWT value in NS control group decreased from baseline (15 g) to around 2 g, which indicated the pain caused by the plantar incision. On the contrary, within the first 4 hours, the PWT values in the other groups were equivalent to the baseline due to the complete analgesic effect caused by ropivacaine. The values decreased to lower than 5 g in the RH group 6 hours after the surgery, or in the RC group 8 hours after the surgery, which indicated the disappearance of the analgesic effect due to the depletion of ropivacaine. On the other hand, the PWT value remained around 10 g in the RQC group 8 hours after the surgery, which indicated a long-lasting analgesic effect caused by slow release of ropivacaine. The PWT values in all groups gradually increased with the time 8 hours after the surgery, as the animals naturally recovered from the surgery. The PWT values in the RQC group remained at relatively high level throughout the whole experiment, exhibiting its sustained analgesic effect in vivo.

Meanwhile, the CPS was also used to assess the pain levels after the surgery and drug injection, and this could also reflect the analgesic effects and duration of different ropivacaine formulations. As shown in Figure 5B, the CPS in the RQC group remained at a very low value (<5) during the whole experiment, which indicated that the formulation almost completely suppressed the pain of surgery and achieved a long-acting analgesia. On the other hand, RH and RC groups showed limited and transient analgesic effects compared with the NS control group, which corresponded with the PWT results described above.

In previous studies, conventional materials such as liposome and polymer were used to prolong the analgesic effect of ropivacaine on postoperative pain model,[45–47] in which the effect of different formulations could last for 24–48 h. In this study,

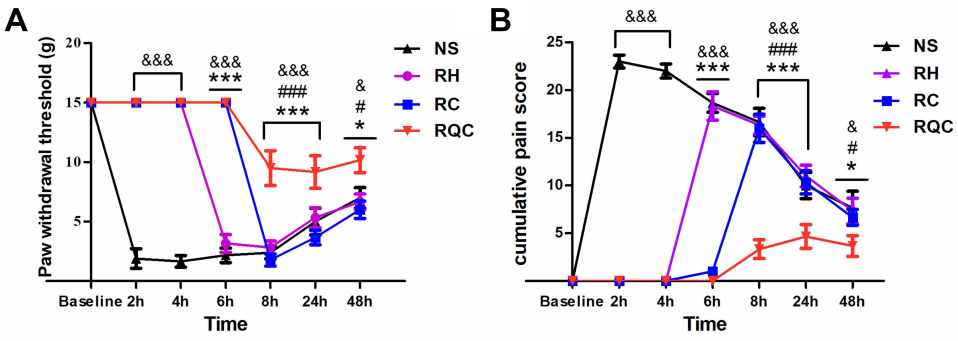

Figure 5 Analgesic effects of different ropivacaine formulations. (**A**) Mechanical PWT and spontaneous hypersensitivity assessed by the von Frey tests. (**B**) CPS results obtained by observing the incisional paw. The statistical significance is shown: $^{\&\&\&}p < 0.001$, and $^{\&}p < 0.05$ (between RQC and NS); $^{***}p < 0.001$, $^{*}p < 0.05$ (between RQC and RH); $^{\#\#\#}p < 0.001$, $^{\#}p < 0.05$ (between RQC and RC) by one-way ANOVA.

the analgesic effect of the RQC formulation reached a duration comparable to those reported in previous researches, providing an alternative slow-release strategy which is simple, effective and biocompatible.

Conclusion

In this study, we report a novel interaction between ropivacaine and the Q11 peptide through π-π stacking, based on which a long-acting ropivacaine nanocrystal formulation was developed. Animal experiments demonstrated that our formulation achieved significantly prolonged anesthetic and analgesic effect compared with RH currently used in clinic. Considering the biocompatibility and biodegradability of Q11 as a peptide-based material totally composed of natural amino acid, the safety of this formulation is also expectable. Since the peptide materials could be easily and reliably obtained by conventional solid-phase synthesis, and the crystallization process could be well-controlled by simply adjusting the pH, this strategy is also facile and cost-effective. However, it should be noted that the effective duration of the current formulation is still not long enough for fulfilling the requirement of treating post-operative pain, which can last for up to 72 hours, so that more works need to be carried out following this direction. Considering the chemical similarity of many other LAs to ropivacaine, their long-acting formulations can be readily developed following the same strategy. On the other hand, considering the prevalence of phenyl ring structure in many drugs and SAPs, more similar strategies based on π-π stacking could be further exploited.

Abbreviations

LAs, local anesthetics; SAPs, self-assembling peptides; RH, ropivacaine hydrocholoride; TEM, transmission electron microscopy; DLS, dynamic light scattering; PDI, polydispersity index; CD, circular dichroism; RC, ropivacaine crystal; RQC, ropivacaine-Q11 crystal; HPLC, high performance liquid chromatography; LC, loading capacity; EE, encapsulation efficiency; SEM, scanning electron microscopy; FT-IR, Fourier transform infrared; XRD, X-ray diffraction; XPS, X-ray photoelectron spectroscopy; ThT, thioflavin-T; DOX, doxorubicin; DQC, DOX-Q11 crystal; CTMR, cutaneous trunci muscle reflex; NS, normal saline; PWT, paw withdrawal threshold; CPS, cumulative pain scores.

Acknowledgments

This work was supported by the National Natural Science Foundation of China (No. 81973274) and Chengdu Science and Technology Bureau (2021-YF05-00917-SN).

Disclosure

The authors report no conflicts of interest in this work.

References

1. Svirskis D, Procter G, Sharma M, et al. A non-opioid analgesic implant for sustained post-operative intraperitoneal delivery of lidocaine, characterized using an ovine model. *Biomaterials*. 2020;263:120409. doi:10.1016/j.biomaterials.2020.120409
2. Hamid HKS, Ahmed AY, Saber AA, et al. Transversus abdominis plane block using a short-acting local anesthetic reduces pain and opioid consumption after laparoscopic bariatric surgery: a meta-analysis. *Surg Obes Relat Dis*. 2020;16:1349–1357.
3. Shah J, Votta-Velis EG, Borgeat A. New local anesthetics. *Best Pract Res Clin Anaesthesiol*. 2018;32:179–185.
4. Cotta BH, Welliver C, Brahmamdam A, et al. Long-acting liposomal bupivacaine decreases inpatient narcotic requirements in men undergoing penile prosthesis implantation. *Turk J Urol*. 2016;42:230–234.
5. Ma P, Li T, Xing H, et al. Local anesthetic effects of bupivacaine loaded lipid-polymer hybrid nanoparticles: in vitro and in vivo evaluation. *Biomed Pharmacother*. 2017;89:689–695.
6. Wei Y, Wu Y, Wen K, Bazybek N, Ma G. Recent research and development of local anesthetic-loaded microspheres. *J Mater Chem B*. 2020;8:6322–6332.
7. Peng F, Zhang W, Qiu F. Self-assembling peptides in current nanomedicine: versatile nanomaterials for drug delivery. *Curr Med Chem*. 2020;27:4855–4881.
8. Acar H, Srivastava S, Chung EJ, et al. Self-assembling peptide-based building blocks in medical applications. *Adv Drug Delivery Rev*. 2017;110–111:65–79.
9. Eskandari S, Guerin T, Toth I, Stephenson RJ. Recent advances in self-assembled peptides: implications for targeted drug delivery and vaccine engineering. *Adv Drug Delivery Rev*. 2017;110–111:169–187.
10. Wu Y, Sadatmousavi P, Wang R, et al. Self-assembling peptide-based nanoparticles enhance anticancer effect of ellipticine in vitro and in vivo. *Int J Nanomed*. 2012;7:3221–3233.
11. Soukasene S, Toft DJ, Moyer TJ, et al. Antitumor activity of peptide amphiphile nanofiber-encapsulated camptothecin. *ACS Nano*. 2011;5(11):9113–9121. doi:10.1021/nn203343z
12. Liu J, Peng F, Kang Y, et al. High-loading self-assembling peptide nanoparticles as a lipid-free carrier for hydrophobic general anesthetics. *Int J Nanomed*. 2021;16:5317–5331.

13. Gelain F, Unsworth LD, Zhang S. Slow and sustained release of active cytokines from self-assembling peptide scaffolds. *J Controlled Release*. 2010;145:231–239.
14. Karavasili C, Panteris E, Vizirianakis IS, Koutsopoulos S, Fatouros DG. Chemotherapeutic delivery from a self-assembling peptide nanofiber hydrogel for the management of glioblastoma. *Pharm Res*. 2018;35:166.
15. Ashwanikumar N, Kumar NA, Saneesh Babu PS, et al. Self-assembling peptide nanofibers containing phenylalanine for the controlled release of 5-fluorouracil. *Int J Nanomed*. 2016;11:5583–5594.
16. Rudra JS, Sun T, Bird KC, et al. Modulating adaptive immune responses to peptide self-assemblies. *ACS Nano*. 2012;6:1557–1564.
17. Franks SJ, Firipis K, Ferreira R, et al. Harnessing the self-assembly of peptides for the targeted delivery of anti-cancer agents. *Mater Horiz*. 2020;7:1996–2010.
18. Yin Y, Wu C, Wang J, et al. A simply triggered peptide-based hydrogel as an injectable nanocarrier of tanshinone IIA and tanshinones. *Chem Commun*. 2017;53:529–532.
19. McClellan KJ, Faulds D. Ropivacaine: an update of its use in regional anaesthesia. *Drugs*. 2000;60:1065–1093.
20. Higuchi H, Adachi Y, Kazama T. Factors affecting the spread and duration of epidural anesthesia with ropivacaine. *Anesthesiology*. 2004;101:451–460.
21. Chou AK, Chiu CC, Chen YW, Wang JJ, Hung CH. Phentolamine reverses epinephrine-enhanced skin antinociception of dibucaine in rats. *Anesth Analg*. 2019;128:1336–1343.
22. Ozyuvaci H, Bilgic B, Ozyuvaci E, et al. Intra-articular injection of tenoxicam in rats: assessment of the local effects on the articular cartilage and synovium. *J Int Med Res*. 2004;32:312–316.
23. Tran PV, Johns ME, McAdams B, et al. Global transcriptome analysis of rat dorsal root ganglia to identify molecular pathways involved in incisional pain. *Mol Pain*. 2020;16:1744806920956480.
24. Pogatzki EM, Vandermeulen EP, Brennan TJ. Effect of plantar local anesthetic injection on dorsal horn neuron activity and pain behaviors caused by incision. *Pain*. 2002;97:151–161.
25. Rudra Jai S, Tian YF, Jung Jangwook P, Collier Joel H. A self-assembling peptide acting as an immune adjuvant. *Proc Natl Acad Sci*. 2010;107:622–627.
26. Votaw NL, Collier L, Curvino EJ, et al. Randomized peptide assemblies for enhancing immune responses to nanomaterials. *Biomaterials*. 2021;273:120825.
27. Li S, Zhang Q, Bai H, et al. Self-assembled nanofibers elicit potent HPV16 E7-specific cellular immunity and abolish established TC-1 graft tumor. *Int J Nanomed*. 2019;14:8209–8219.
28. Marchut AJ, Hall CK. Side-chain interactions determine amyloid formation by model polyglutamine peptides in molecular dynamics simulations. *Biophys J*. 2006;90:4574–4584.
29. Ranganathan D, Haridas V, Gilardi R, Karle IL. Self-assembling aromatic-bridged serine-based cyclodepsipeptides (serinophanes): a demonstration of tubular structures formed through aromatic π–π interactions. *J Am Chem Soc*. 1998;120:10793–10800.
30. Jung JP, Nagaraj AK, Fox EK, et al. Co-assembling peptides as defined matrices for endothelial cells. *Biomaterials*. 2009;30:2400–2410.
31. Zhang C, Xue X, Luo Q, et al. Self-assembled Peptide nanofibers designed as biological enzymes for catalyzing ester hydrolysis. *ACS Nano*. 2014;8:11715–11723.
32. Li R, Liu K, Huang X, et al. Bioactive materials promote wound healing through modulation of cell behaviors. *Adv Sci*. 2022;9:2105152.
33. Feng Z, Su Q, Zhang C, et al. Bioinspired nanofibrous glycopeptide hydrogel dressing for accelerating wound healing: a cytokine-free, M2-type macrophage polarization approach. *Adv Funct Mater*. 2020;30:2006454.
34. Collier JH, Messersmith PB. Enzymatic modification of self-assembled peptide structures with tissue transglutaminase. *Bioconjugate Chem*. 2003;14:748–755.
35. Hunter CA, Singh J, Thornton JM. π-π interactions: the geometry and energetics of phenylalanine-phenylalanine interactions in proteins. *J Mol Biol*. 1991;218:837–846.
36. Nguyen Thi Thanh C, Nguyen Bich N, Van ML. Hydrogen-bonded chains in three cis-dichloridoplatinum (II) complexes bearing piperidine and amine ligands. *Acta Crystallogr Sect C*. 2014;70:297–301.
37. Yuasa J, Mitsui A, Kawai T. π–π* Emission from a tetrazine derivative complexed with zinc ion in aqueous solution: a unique water-soluble fluorophore. *Chem Commun*. 2011;47:5807–5809.
38. Chen Y, Xing Z, Liao D, Qiu F. Neglected hydrophobicity of dimethanediyl group in peptide self-assembly: a hint from amyloid-like peptide GNNQQNY and its derivatives. *J Phys Chem B*. 2018;122:10470–10477.
39. Foley PL, Ulery BD, Kan HM, et al. A chitosan thermogel for delivery of ropivacaine in regional musculoskeletal anesthesia. *Biomaterials*. 2013;34:2539–2546.
40. Cho Y, Ivanisevic A. TAT peptide immobilization on gold surfaces: a comparison study with a thiolated peptide and alkylthiols using AFM, XPS, and FT-IRRAS. *J Phys Chem B*. 2005;109:6225–6232.
41. Li X, Wei Y, Wen K, et al. Novel insights on the encapsulation mechanism of PLGA terminal groups on ropivacaine. *Eur J Pharm Biopharm*. 2021;160:143–151.
42. Yin Q, Zhang W, Ke B, Liu J, Zhang W. Lido-OH, a hydroxyl derivative of lidocaine, produced a similar local anesthesia profile as lidocaine with reduced systemic toxicities. *Front Pharmacol*. 2021;12:1933.
43. Tzeng J-I, Chiu -C-C, Wang -J-J, Chen Y-W, Hung C-H. Isobolographic analysis of the cutaneous antinociceptive interaction between bupivacaine co-injected with serotonin in rats. *Pharmacol Rep*. 2017;69:846–850.
44. Kao HW, Lin YY, Gwathney WJ, Hong K. Formulation and evaluation of multilamellar vesicles ropivacaine in pain management. *Int J Nanomed*. 2019;14:7891–7901.
45. Davidson EM, Haroutounian S, Kagan L, et al. A novel proliposomal ropivacaine oil: pharmacokinetic-pharmacodynamic studies after subcutaneous administration in pigs. *Anesth Analg*. 2016;122:1663–1672.
46. Renno CC, Papini JZB, Cereda CMS, et al. Preclinical evaluation of ropivacaine in 2 liposomal modified systems. *Anesth Analg*. 2019;129:387–396.
47. Lu L, Zhang W, Wu X, et al. A novel ropivacaine-loaded in situ forming implant prolongs the effect of local analgesia in rats. *Arch Med Sci*. 2013;9:614–621.